2016

Automatic Mode Switching for A Multi-functional Variable Refrigerant Flow System

Liujia Dong
The University of Texas at Dallas, United States of America, lxd122030@utdallas.edu

Yaoyu Li
The University of Texas at Dallas, United States of America, yxl115230@utdallas.edu

Timothy I. Salsbury
Johnson Controls, Inc., timothy.i.salsbury@jci.com

John M. House
Johnson Controls, Inc., john.m.house@jci.com

Automatic Mode Switching for A Multi-functional Variable Refrigerant Flow System

Liujia Dong[1]*, Yaoyu Li[1], Timothy I. Salsbury[2], John M. House[2]

[1]The University of Texas at Dallas
800 W. Campbell Rd., Richardson, TX 75080, USA
Liujia.Dong@utdallas.edu; yaoyu.li@utdallas.edu

[2]Johnson Controls, Inc.
507 E. Michigan St., Milwaukee, WI 53201, USA
Timothy.I.Salsbury@jci.com; John.M.House@jci.com

* Corresponding Author

ABSTRACT

The Multi-functional Variable Refrigerant Flow (MFVRF) system is designed to realize simultaneous heating and cooling for temperature regulation of individual zones by allowing the heat exchangers of both indoor and outdoor units to operate as an evaporator or condenser. It is thus desirable to use measurements readily available on the MFVRF system to determine switching between different modes, which involves reversing the mode of indoor unit (IDU), and/or outdoor unit (ODU) heat exchangers (HX), as well as realizing smooth transition for such mode changes. In this study, an automatic mode switching strategy is proposed for a multi-zone MFVRF system, involving both IDU and ODU mode switching. Turning on or off an IDU is determined by the zone temperature with respect to the preset hysteresis band about the temperature setpoint. The cooling mode (CM) or heating mode (HM) can be realized by opening the CM or HM related valves within a specified time duration while closing the valves for the opposite mode. The IDU fan is off if the IDU is neither in CM or HM. For the ODU-HX, a thermodynamic analysis is performed for the air-side and refrigerant-side characteristics for load conditions that need mode switching. It reveals that the air-side temperature differential becomes significantly smaller and the system COP dramatically reduced if the ODU-HX works in an inappropriate mode. Therefore, the ODU-HX air-side temperature differential is proposed as the thresholding variable for determining ODU-HX mode switching. Furthermore, two bumpless transfer schemes are applied to realize smooth mode switching with reasonable transient duration. To evaluate the proposed cost-effective and model-free mode switching strategy, simulation study is performed with a Modelica based dynamic simulation model of a four-zone MFVRF system. Simulation results validate the effectiveness of the proposed strategy as well as the bumpless transfer performance.

1. INTRODUCTION

Variable refrigerant flow (VRF) air conditioning systems feature multi-split ductless configurations using one outdoor unit (ODU) and multiple indoor units (IDU) (Park *et. al*, 2001). With variable capacity compressor and electronic expansion valve (EEV), the VRF systems can control the refrigerant flow to the evaporators of multiple IDUs, thus enabling operation of individual zoning with variable capacities. VRF systems offer many advantages, such as elimination of duct loss of air distribution, design and installation flexibility, compactness, integrated controls, quiet operation and reduced maintenance cost (Goetzler 2007). The so-called Multi-functional VRF (MFVRF) system realizes simultaneous heating and cooling via the so-called Mode Change Unit (MCU) which is effectively a valve array that regulates the refrigerant flows through the IDUs (Aynur 2010, Xia *et al.* 2002, Masuda 1991) to achieve five possible operation modes: i) cooling-only; ii) heating-only; iii) cooling-dominated; iv) heating-dominated; and v) heat recovery (Hai *et. al.* 2006, Shi *et. al.* 2003, Xia *et al.* 2004).

The multi-split nature and flexibility in configuration make VRF systems more challenging for controls. Simple control strategies have been evaluated, e.g. by Masuda *et al*. (1991), Park *et al*. (2001), Xia *et al*. (2002), Xia *et al.* (2003), Choi and Kim (2003), Hu and Yang (2005), Hai *et al*. (2006) and Zhou *et al*. (2008), with performance evaluated for different operation scenarios. Aynur *et al*. (2006) present a field study on both individual and master control methods for a multi-split VRF system in an actual building. Joo *et al*. (2011) study the performance of

various modes of a MFVRF system with the four IDU's at partial load conditions. Shi *et al*. (2003) developed a fluidic network model to simulate the performance of a three-pipe VRF with two IDU's. Wu *et al*. (2005) present a self-tuning fuzzy control strategy with experimental validation. Lin and Yeh (2007) develop a multi-input-multi-output (MIMO) feedback control scheme for a three-evaporator air conditioning system. Elliott *et al*. (2013) presents a decentralized model predictive control (DMPC) for a multi-evaporator HVAC system. The pressure and cooling setpoints are optimized by a DMPC that minimizes tracking error and energy consumption. Jain *et al*. (2014) present partially linear quadratic (LQ) decentralized control architecture for large-scale VRF systems.

Under certain ambient and load conditions, the IDU's and ODU of an MFVRF system need to switch the operating mode of their respective heat exchangers to achieve the following objectives: 1) the IDU heat exchanger works as an evaporator for cooling mode or as a condenser for heating mode, and 2) the ODU heat exchanger works as a condenser for a cooling dominant mode or as an evaporator for a heating dominant mode. In order to realize these mode switches, the MCU valves are used to regulate the directions of the refrigerant flow through the IDU's, while the ODU control valves are used to reverse the refrigerant flow to switch the operating mode of the ODU heat exchangers. Switching of IDU heat exchanger mode is relatively straightforward as the IDU zone temperature can be an easy and effective variable to trigger such mode changes. The switching of ODU heat exchanger role is far more complicated. Inappropriate ODU heat exchanger mode setting would lead to a low coefficient of performance (COP) for the system, and therefore in principle, the online COP evaluation should be sufficient for determining such mode switch. However, COP evaluation requires enthalpy measurements which need installation of expensive sensors. Therefore, it would be highly beneficial for practical implementation if the mode switching can be based on measurement(s) readily available on commercial VRF systems.

In this study, we develop a cost-effective and model-free mode switching strategy for both IDU and ODU heat exchanger operations in MFVRF systems. Turning on or off an IDU is determined by the zone temperature with respect to the preset hysteresis band about the temperature setpoint. The cooling mode (CM) or heating mode (HM) can be realized by opening the CM or HM related valves within a specified time duration while closing the valves for the opposite mode. The IDU fan is off if the IDU is neither in CM or HM. For ODU mode switching, the heat exchanger air-side temperature differential is proposed as the threshold variable, based on a thermodynamic analysis for the transitional scenarios between heating dominant and cooling dominant modes. In order to achieve smooth transition during mode switching, two bumpless transfer techniques are applied: the Conditioning Bumpless Transfer (CBT) by Hanus *et al.* (1996) and the Linear Quadratic Bumpless Transfer (LQBT) by Turner and Walker (2000) The proposed mode switching strategy is evaluated with a Modelica based dynamic simulation model of a four-zone MFVRF system recently developed by the authors (Dong *et al*. 2016), which is based on Dymola (Dassault Systems, 2015) and TIL Library (Richter 2008; TLK-Thermo, 2014a).

The rest of this paper is organized as follows. Section 2 describes the Modelica based dynamic simulation model of MFVRF system. Section 3 presents the mode switch control logic for IDU and ODU of multi-functional VRF system. The CBT and LQBT schemes are described in Section 4, along with their realizations for the MFVRF mode switching operation. Simulation results are presented in Section 5, and Section 6 concludes this paper with a discussion of possible future work.

2. MFVRF SYSTEM MODELING

Fig. 1 shows the schematic of the four-zone MFVRF system considered in this study (Dong *et al*. 2016), which consists of one ODU, one MCU and four IDUs. The ODU includes a variable speed compressor, a bypass valve (BPV), a heat exchanger, an EEV (EEV_O), and mode-control solenoid valves (C_{OL}, C_{OR} and H_O). The BPV inlet is connected to the compressor, and the two outlets of BPV are connected to C_{OL} and the heating-mode valves in MCU respectively. The BPV can distribute the refrigerant flow to the two branches. When the ODU HX is operated as condenser (under higher cooling demand), valves C_{OL} and C_{OR} are opened while H_O and EEVo are closed. For each zone, the zone temperature is regulated by the mass flow rate of its IDU fan with a proportional-integral (PI) controller. When the heat exchanger is working as an evaporator, either for IDU or ODU, the superheat is regulated by the EEV opening with a PI controller. For cooling dominant cases, the compressor suction pressure (P_{CS}) is regulated by the compressor speed with a PI controller. For heating dominant cases, the compressor discharge pressure (P_{CD}) is regulated by the compressor speed with another PI controller. To evaluate the proposed control strategy, a Modelica based dynamic finite volume simulation model is developed, using Dymola 2014, TIL Library 3.2 and TIL Media Library 3.2. More details on the system configuration and operational mechanisms can be found in Dong *et al.* (2016).

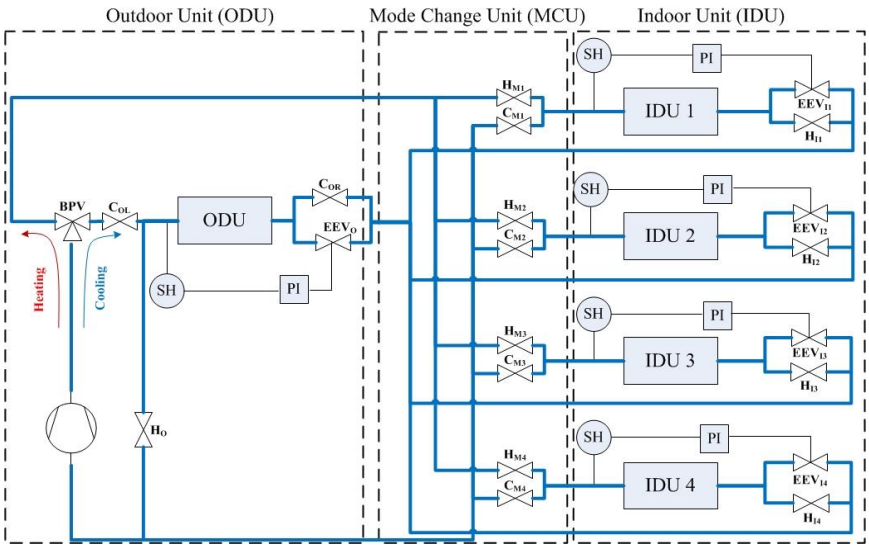

Figure 1. Schematic diagram of a four-zone MFVRF system.

3. MODE SWITCHING FOR MULTI-FUNCTIONAL VRF SYSTEM

Under certain change of ambient and load conditions, the MFVRF system is expected to switch between the aforementioned operations modes. Assume that the zone temperature control for the i-th IDU adopts a hysteresis band as $\left[T_{ic}^{\min}, T_{ic}^{\max}\right]$ and $\left[T_{ih}^{\min}, T_{ih}^{\max}\right]$ for cooling and heating, respectively. $T_{ic}^{\max} > T_{ic}^{sp} > T_{ic}^{\min} > T_{ih}^{\max} > T_{ih}^{sp} > T_{ih}^{\min}$ for practical operation. The supervisory logic for mode switching is proposed as shown in Fig. 2.

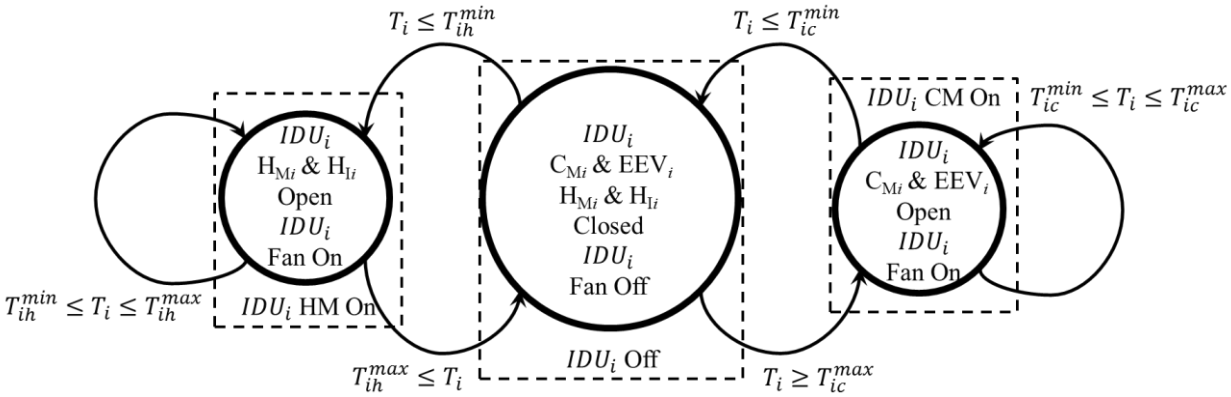

Figure 2. Control Logic of Mode Switching for IDU Operation

When the zone is operated in cooling mode (CM), all related CM valves (i.e. $C_{M,i}$ and $EEV_{I,i}$) of the IDU-i are open and heating mode (HM) valves (i.e. $H_{M,i}$ and $H_{I,i}$) are closed. When the CM is turned off, the CM valves are closed. After the CM is turned off, the i-th IDU will be shut off. At the refrigerant side, all valves of IDU are fully closed, and the mass flow rate of refrigerant is zero. At the air side, the IDU fan will be turned off as well. When the zone is operated in HM, all HM related valves (i.e. $H_{M,i}$ and $H_{I,i}$) are open, and CM related valves (i.e. $C_{M,i}$ and $EEV_{I,i}$) are closed. If the HM is off, the HM related valves (i.e. $H_{M,i}$ and $H_{I,i}$) are closed. Also the IDU fan will be turned off.

For the ODU mode switching, the ODU air-side temperature differential is selected as the measurement for triggering the mode switching. In order to justify the use of ODU air-side temperature differential as the indicator variable for ODU mode switching, several cases of 2H2C mode are first simulated, in which the IDU-1 and IDU-2 are operated in HM and IDU-3 and IDU-4 are operated in CM. Room temperature responses to a cooling load that decreases linearly from 2400W cooling load to 400W, 200W, and 0W cooling load over 1000 seconds are shown in Fig. 3(a) as Cases 1, 2 and 3, respectively. For the ODU-HX, the air inlet temperature is fixed at the ambient 20°C, while the air outlet temperature approaches closer and closer to 20°C under reducing cooling load in IDU-3. The

ODU air outlet temperature, COP, and compressor power and speed are summarized in Table 1, which reveals the trend of decreasing COP.

TABLE 1: Evaluation of Several 2H2C Operations with ODU-HX as Condenser

Simulation Case	Case 1	Case 2	Case 3
ODU-HX air outlet temp. (°C)	21.57	20.87	20.12
COP	0.78	0.65	0.59
Compressor power (W)	799.9	666.3	622.3
Compressor speed (Hz)	31.23	26.11	25.34

Fig. 3(b) shows the *T-s* diagram for the refrigerant cycle of 2H2C mode under several scenarios of reduction in IDU-3 cooling load, plotted with the DaVE software (TLK-Thermo 2014b) developed by TLK-Thermo. The temperature difference at the ODU-HX refrigerant side decreases with the aforementioned change, which is correlated to the decreasing temperature difference at the air side as well as the system COP. Therefore, a decreasing temperature difference at the air side or refrigerant side can be a candidate predictive variable for mode switching of ODU HX.

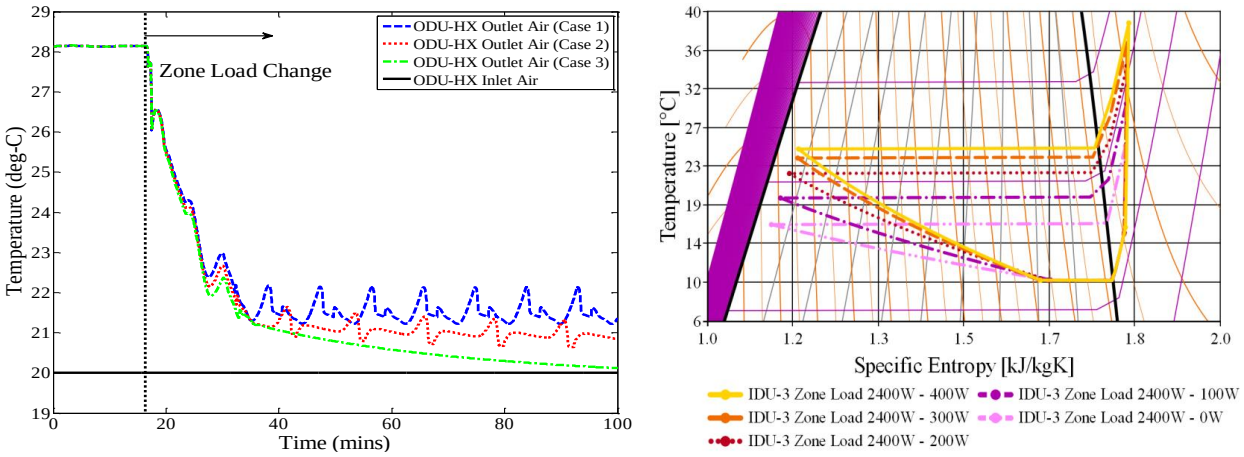

(a) ODU-HX air-side inlet and outlet temperature (b) *T-s* diagram for refrigeration cycle

Figure 3. Simulations of 2H2C mode with ODU HX as condenser under different load conditions.

A similar study is conducted when the ODU HX works as evaporator. The system is operated in 3H1C mode, in which IDU-1 through IDU-3 are in HM, while IDU-4 is in CM. Room temperature responses to a cooling load that decreases linearly from 2700W heating load to 400W, 200W, and 0W heating load over 1000 seconds are shown in Fig. 4(a) as Cases 1, 2 and 3, respectively. For the three cases, the ODU outlet air temperature becomes 14.3°C, 15.9°C and 17.7°C, respectively, closer and closer to the ambient 20°C. The root cause for the observations in Figure 4(a) can be explained with the *T-s* diagrams for the refrigerant cycle of these scenarios in Fig. 4(b). As the heating load of IDU-3 reduces, the evaporator SH keeps reducing. Therefore, the air-side temperature difference as well as the ODU-HX SH can be used as indicator for the mode switching from evaporator to condenser. The above simulation cases reveals that the role of ODU-HX for efficient operation of the MFVRF system can be determined by the air-side temperature difference of the ODU HX ($\Delta T_{ODU} = T_{air,out} - T_{air,in}$), i.e. by the virtue of a preset threshold ($-\varepsilon_{\min}$, $\varepsilon_{\max}$). If $\Delta T_{ODU} \geq \varepsilon_{\max}$, the ODU works as condenser, the compressor suction pressure is controlled. If $\Delta T_{ODU} \leq -\varepsilon_{\min}$, the ODU works as evaporator, the compressor discharger pressure is controlled. The state transition diagram for the ODU-HX mode switching is shown in Fig. 5.

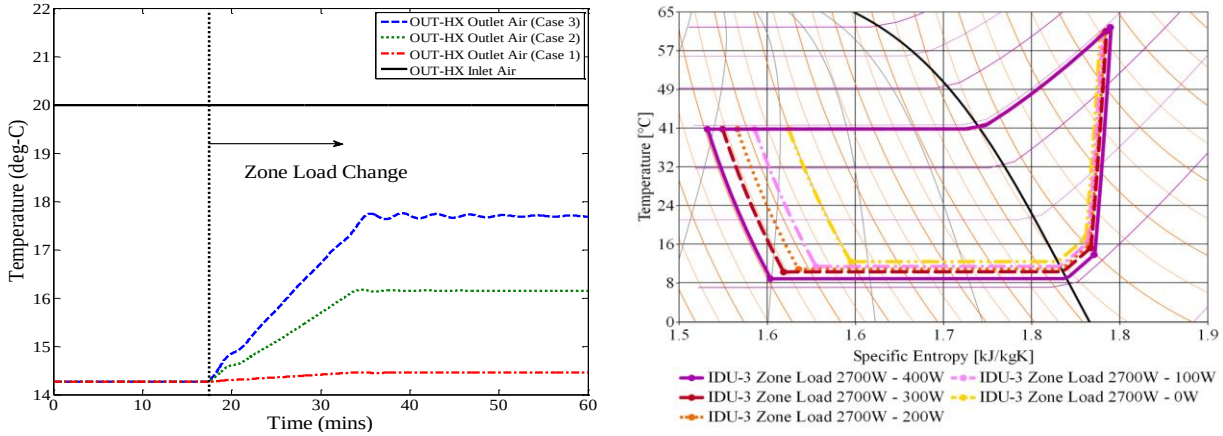

(a) ODU-HX air-side inlet and outlet temperature (b) *T-s* diagram for refrigeration cycle.

Figure 4. Simulations of 3H1C mode with ODU HX as evaporator under different load conditions.

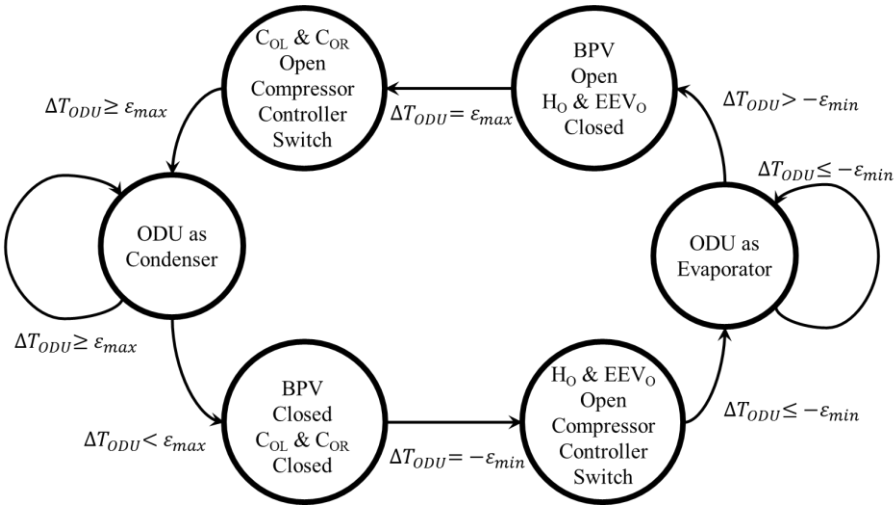

Figure 5. State Transition Diagram for Mode Switching of ODU-HX Operation.

4. BUMPLESS TRANSFER BETWEEN COMPRESSOR SUCTION/DISCHARGER PRESSURE CONTROLLERS

For ODU-HX mode switching, it is necessary to switch between two compressor pressure controls: the suction and discharge pressure setpoint controls as shown in Fig. 6. Ω_{comp} is the compressor speed command. Undesirable transients or even instability may occur when switching between these two pressure setpoint control loops due to discontinuities in two states and also controller outputs. It is ideal to achieve a smooth transition without stopping the compressor. Two bumpless transfer techniques have been considered in this study: the CBT techniques for PI control (Hanus *et al*. 1996, Peng *et al*. 1996) and LQBT (Turner and Walker, 2000), as illustrated in Fig. 7.

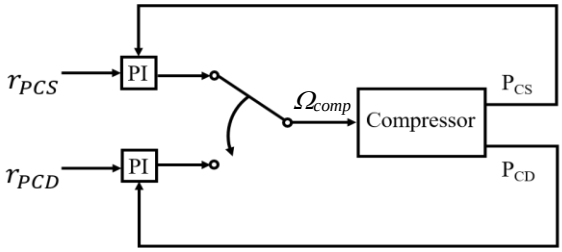

Figure 6. Illustrative Block Diagram for Switching between Compressor Pressure Controllers.

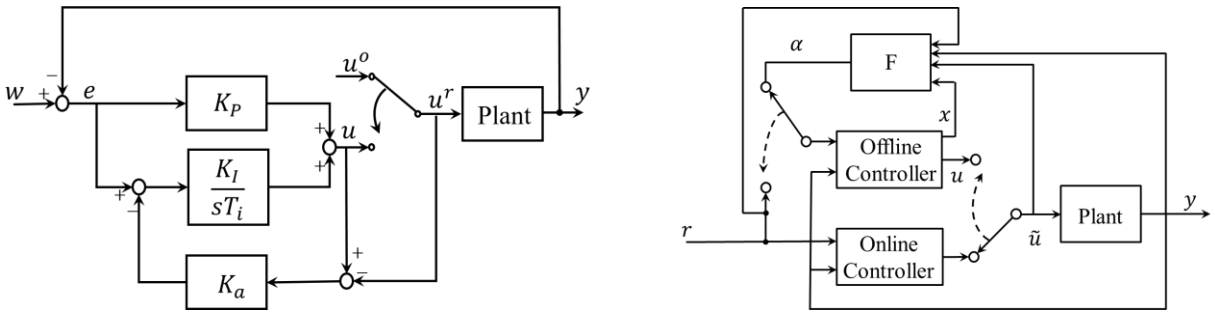

(a) Conditioned Transfer **(**b**)** Linear Quadratic Bumpless Transfer

Figure 7. Block Diagrams of Two Bumpless Transfer Schemes

The conditioned transfer technique is first considered when the simple PI controllers are used, as shown in Fig. 7(a). The discrete-time state-space realization of a typical PI controller is given by (Peng *et al*. 1996)

$$v(t+1) = v(t) + K_I\{w(t) - y(t)\} \tag{1a}$$

$$u(t) = v(t) + K_p\{w(t) - y(t)\} \tag{1b}$$

where K_P and K_I are the proportional and integral gains, respectively, v is the integration state, and $w - y = e$ is the control error. The conditioned transfer is realized based on:

$$w^r(t-1) = w(t-1) + \frac{u^r(t-1) - u(t-1)}{K_p} \tag{2a}$$

$$v^r(t) = v^r(t-1) + K_I\{w^r(t-1) - y(t-1)\} \tag{2b}$$

$$u^r(t) = v^r(t) + K_p\{w(t) - y(t)\} \tag{2c}$$

where w^r is the so-called auxiliary inputs, and u^r is the actual control variables as opposed to the desired variable u. States v are obtained with the new input w^r. At time instant t–1, the desired variable $u(t-1)$ are known, the accrual variable $u^r(t-1)$ are measured, and the prior values of the reference variable $w^r(t-1)$ can be calculated. These prior values are used to update the adequate states $v^r(t)$, the present measures of the outputs $y(t)$, and the present actual values of the references $w(t)$ are used to compute $u(t)$, based on the following equations:

$$w(t) = y(t) + \frac{u(t) - v(t)}{K_p} \tag{3}$$

$$v(t) = v(t-1) + \frac{K_I}{K_a}\{u(t-1) - v(t-1)\} \tag{4}$$

$$v^r(t) = v^r(t-1) + \frac{K_I}{K_a}\{u^r(t-1) - v^r(t-1)\} \tag{5}$$

$$u(t) = v^r(t) + K_p\{w(t) - y(t)\} \tag{6}$$

The LQ bumpless transfer method, as shown in Fig. 7(b), is based on minimization of the difference between the online control signal and offline control signal, as well as the error signal and the signal which drives the offline controller. The LQ bumpless transfer is based on the following cost function (Turner and Walker, 2000):

$$J(u,\alpha,T) = \frac{1}{2}\int_0^T \left[z_u(t)'W_u z_u(t) + z_e(t)'W_e z_e(t)\right]dt + \frac{1}{2}z_u(T)'Pz_u(T) \tag{7}$$

where $z_u = u(t) - \tilde{u}(t)$ and $z_e = \alpha(t) - \tilde{e}(t)$. $\tilde{u}(t)$ and $\tilde{e}(t)$ are the online control signal and error signal, respectively. $\alpha(t)$ is the signal produced by the feedback gain which drives the offline controller. W_u and W_e are constant positive-definite weighting matrices. z_u is the difference between the two control signals. For the offline controller is being driven by the signal $\alpha(t)$, with the state-space realization as

$$\begin{cases} \dot{x} = Ax + B\alpha \\ u = Cx + D\alpha \end{cases} \tag{8}$$

Then Eq. (7) becomes

$$J(u,\alpha,T)=\frac{1}{2}\int_0^T[(Cx+D\alpha-\tilde{u})'W_u(Cx+D\alpha-\tilde{u})+(\alpha-\tilde{e})'W_e(\alpha-\tilde{e})]dt+\frac{1}{2}z_u(T)'Pz_u(T) \tag{9}$$

By introducing Lagrange multiplier $\lambda(t)\in\Re^n$, Eq. (9) becomes

$$\tilde{J}=\frac{1}{2}\int_0^T\left[H(t)-\lambda(t)'\dot{x}\right]dt+\phi(T) \tag{10}$$

with $\phi(T)=\frac{1}{2}z_u(T)'Pz_u(T)$. The Hamiltonian is given by

$$H(t)=\frac{1}{2}\left[(Cx+D\alpha-\tilde{u})'W_u(Cx+D\alpha-\tilde{u})+(\alpha-\tilde{e})'W_e(\alpha-\tilde{e})\right]+\lambda'(Ax+B\alpha) \tag{11}$$

Applying the first-order necessary conditions for a minimum of the cost function (9) yields

$$\frac{\partial H}{\partial\lambda}=Ax+B\alpha \tag{12}$$

$$\frac{\partial H}{\partial x}=A'\lambda+C'W_uCx-C'W_u\tilde{u}+C'W_uD\alpha \tag{13}$$

$$\frac{\partial H}{\partial\alpha}=\left(D'W_uD+W_e\right)\alpha+D'W_uCx+B'\lambda-D'W_u\tilde{u}-W_e\tilde{e} \tag{14}$$

Using the expression for α in the state and co-state equations,

$$\begin{bmatrix}\dot{x}\\ \dot{\lambda}\end{bmatrix}=\begin{bmatrix}\tilde{A} & \tilde{B}\\ -\tilde{C} & -\tilde{A}\end{bmatrix}\begin{bmatrix}x\\ \lambda\end{bmatrix}+\begin{bmatrix}-B\Delta W_e\\ C'W_uD\Delta W_e\end{bmatrix}\tilde{e}+\begin{bmatrix}-B\Delta D'W_u\\ C'W_u(I+D\Delta D'W_u)\end{bmatrix}\tilde{u} \tag{15}$$

where $\tilde{A}=A+B\Delta D'W_uC$, $\tilde{B}=B\Delta B'$, $\tilde{C}=C'W_u(I+D\Delta D'W_u)C$, $\Delta=-(D'W_uD+W_e)^{-1}$. Assuming $(\tilde{A},\tilde{B})$ is stablizable, $(\tilde{A},\sqrt{\tilde{C}})$ is detectable, and the terminal solution to the Riccati differential equation is positive semi-definite. In this study, the infinite-horizon solution is adopted for ease of implementation, which is based on solving for the following algebraic Riccati equation:

$$\Pi\tilde{A}+\tilde{A}'\Pi+\Pi\tilde{B}\Pi+\tilde{C}=0 \tag{16}$$

The solution to (16) can be used to obtain α as

$$\alpha=\Delta\begin{bmatrix}(B'\Pi+D'W_uC)'\\ -D'W_u+C'M(C'W_u+C'W_uD\Delta D'+\Pi B\Delta D'W_u)'\\ (-W_e+B'M(C'W_uD\Delta W_e+\Pi B\Delta W_e))'\end{bmatrix}\begin{bmatrix}x\\ \tilde{u}\\ \tilde{e}\end{bmatrix} \tag{17}$$

with $M=(\tilde{A}'+\Pi\tilde{B})^{-1}$. Therefore, the synthesize feedback matrix F can be calculated by solving the algebraic Riccati equation and the state and co-state equations. The signal $\alpha(t)$ produced by F is the signal driven the offline controller to achieve bumpless transfer.

5. SIMULATION OF MODE SWITCHING STRATEGY FOR MFVRF SYSTEMS

Based on the mode switching strategy proposed in Section 3, it is proposed to use the temperature difference between the inlet and outlet air temperature to trigger the mode switching for the ODU HX. For example, for the ODU HX working as condenser, if the air-side temperature difference falls below 5°C for a specific time period (e.g. 5 minutes), the ODU HX is switched to evaporator by manipulating the appropriate valves.

An ODU-HX mode switching scenario is first simulated with the system operation changed from the 2H2C to 3H1C mode. The ambient temperature and relative humidity are set as 20°C and 20 %RH, respectively. For IDU-3, a 300-second ramp change is applied, from 2800W heating load to 7000W cooling load. For the 2H2C mode, the initial zone temperature of the heating-operation units is set to be 20°C, and the temperature setpoint is 23°C. The cooling-operation units' initial temperature is 29°C, and the temperature setpoint is 27°C. For the 3H1C mode, due to the load change of the IDU-3, the unit becomes heating operation unit, and the new temperature setpoint is 22°C. The

zone temperature regulation for overall simulation time period is shown in Fig. 8. The load change profile, ODU air side inlet and outlet temperature, IDU and ODU mode change valves operation during ODU role-switching period results are shown in Fig. 9. The ODU SH and IDU4 SH with corresponding EEV opening are shown in Fig. 10.

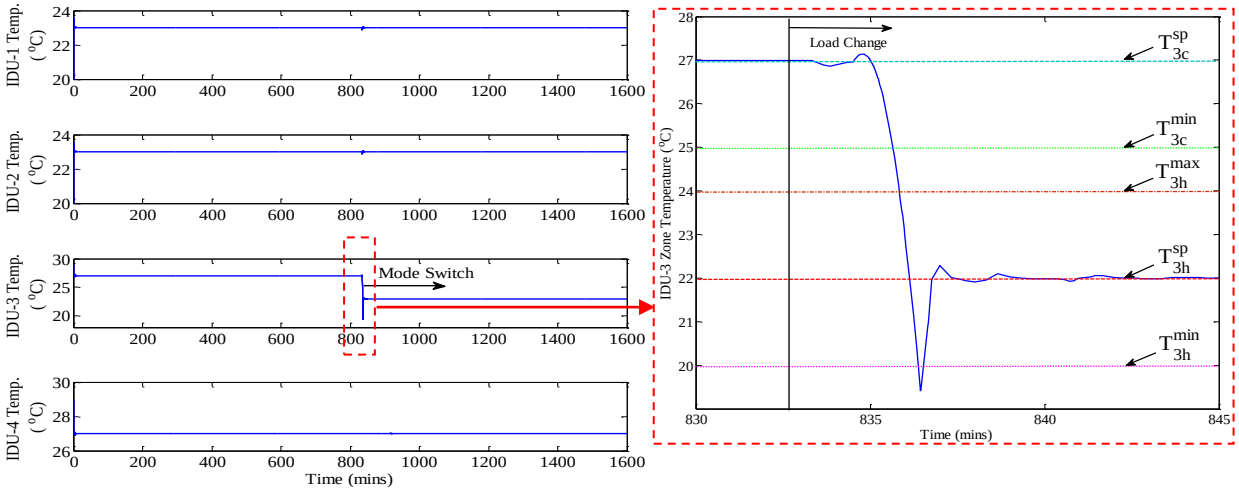

Figure 8. Zone temperature profiles for the switching from 2H2C to 3H1C mode.

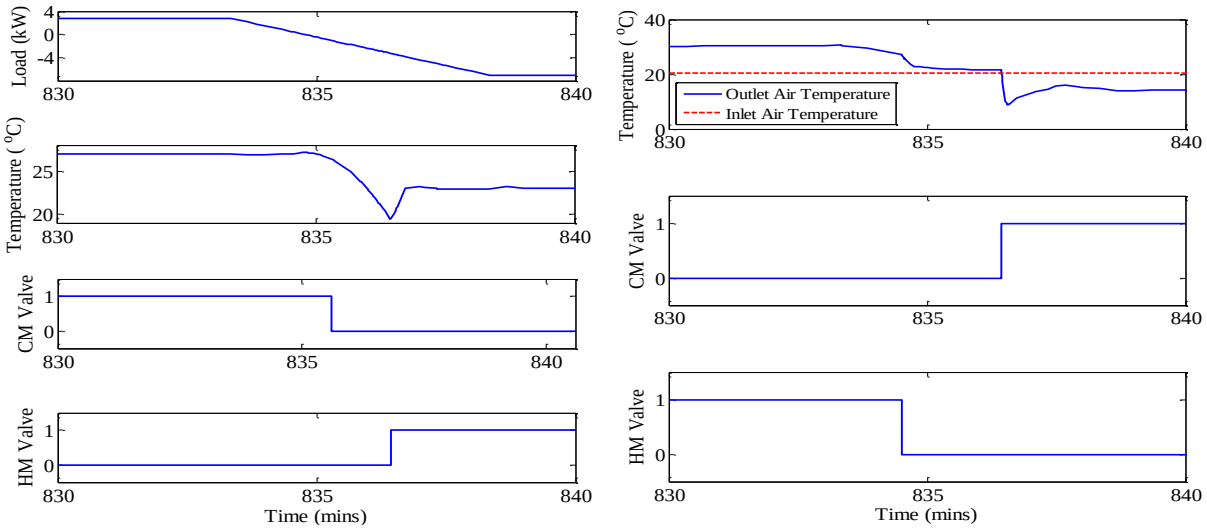

Figure 9. IDU3 load change, IDU3 mode-change valve actions, ODU inlet/outlet air temperatures, and ODU mode change valve actions for the switching from 2H2C to 3H1C mode.

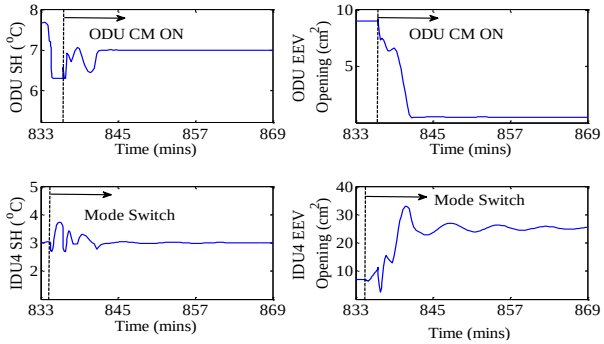

Figure 10. SH and EEV opening of ODU-HX and IDU4 HX for the switching from 2H2C to 3H1C mode.

Both bumpless transfer schemes are applied for the mode switching process. For the CBT case, K_P, K_I and K_a are 10, 0.006 and 1.5, respectively. For the LQBT case, W_u and W_e are selected as 10 and 0.1, respectively. The compressor

speed and compressor suction and discharge pressure are plotted in Fig. 11. After the controller switching, the compressor speed converges to 123.6 Hz in the 3H1C mode. To evaluate the transient performance, the 2% settling time is 17 minutes, 12 minutes and 6 minutes, for the bumped transfer, the CBT and LQBT, respectively. The integral absolute error (IAE) is calculated for 17 minutes of operation from the switching instant, which is 573.2, 548.6 and 515.3, respectively, for the bumped transfer, CBT and LQBT cases. The compressor speed controls the suction and discharge pressure setpoint before and after the switching, shown as Regions 1 and 2, respectively in the figure. The pressure profiles show negligible difference among the three scenarios.

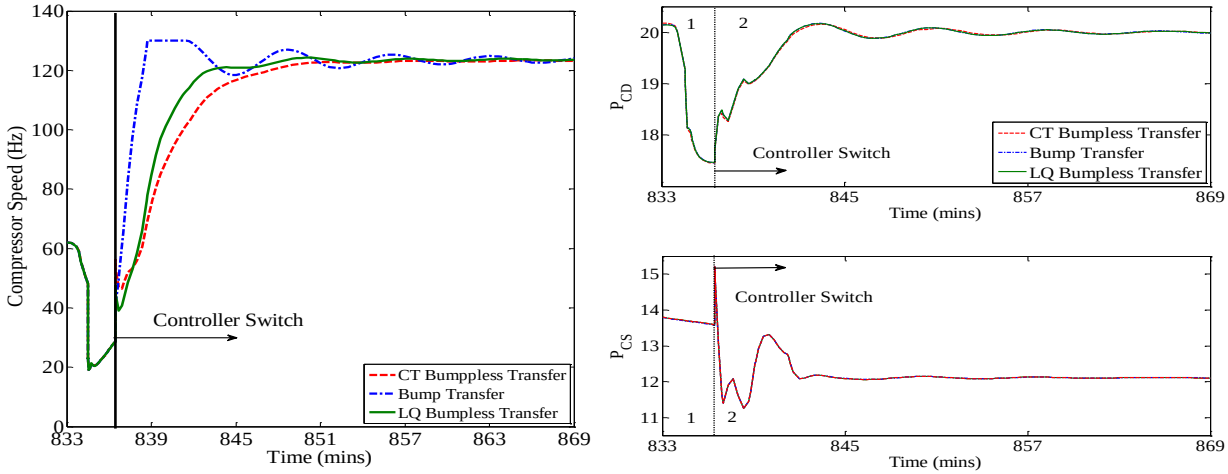

Figure 11. Compressor speed and pressure profiles for the switching from 2H2C to 3H1C mode.

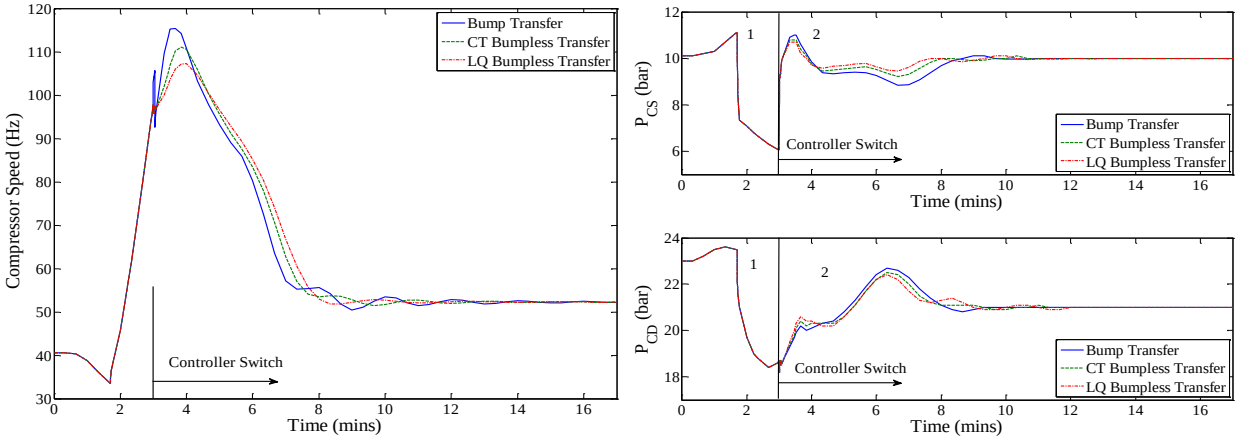

Figure 12. Compressor speed and pressure profiles for the switching from 3H1C to 2H2C mode.

Switching of ODU-HX from evaporator to condenser mode is then simulated with a scenario of switching from 3H1C to 2H2C mode. With the aforementioned ambient condition, the MFVRF starts with IDU-1, IDU-2 and IDU-3 in heating and IDU-4 in cooling. Then IDU-3 is applied a 5-minute ramp change from 2700W cooling load to 7000W heating load. Fig. 12 shows the compressor speed and pressure profiles. For the 2H2C mode, the compressor speed converges to 52.3 Hz. The 2% settling times for the bumped transfer, CBT and LQBT are 7, 6 and 4.8 minutes, respectively. The IAE's within 7 minutes from mode switching are 241.5, 200.6 and 178.2, respectively, for the bumped transfer, CBT and LQBT. Again, the pressure profiles show negligible difference among three cases.

6. CONCLUSIONS

An automatic mode switching scheme is proposed for multi-zone MFVRF system, along with the bumpless transfer schemes to achieve smooth transition between the compressor pressure control loops. For the ODU-HX mode switching, the air-side temperature differential is proposed as the thresholding variable, justified with simulation based study. A simulation study is performed with a Modelica dynamic simulation model of a four-zone MFVRF system for switching between 2H2C and 3H1C modes. The zone temperature control is regulated with the corresponding IDU fan mass flow rate. The simulation results validate the effectiveness of the proposed strategy,

with CBT and LQBT both achieving significant improvement in mode switching transient. LQBT achieves better performance, with the tradeoff of more complexity. The proposed mode switching strategy is a model-free scheme based on a readily available sensor on commercial MFVRF systems, which makes itself a cost-effective solution for such systems in field operation. The future work include the investigation of using EEV to regulate IDU zonal temperature setpoint and the robustness of the proposed method under more realistic conditions for the ODU-HX .

REFERENCES

Park, Y.C., Kim, Y.C., Min, M.K. 2001, "Performance analysis on a multi-type inverter air conditioner," *Energy Conv. Mgmt.,* **42**(13) (2001) 1607–1621.

Aynur, T.N. 2010, "Variable refrigerant flow systems: A review," *Energy and Buildings* **42**(2010), 1106-1112.

Goetzler, W. 2007, "Variable refrigerant flow systems," *ASHRAE Journal*, **49** (4) (2007) 24–31.

Xia, J., Winandy, E., Georges, B., Lebrun, J. 2002, "Testing methodology for VRF systems," *9th Int. Refri. Air Cond. Conf.*

Masuda, M., Wakahara, K., Matsui, K. 1991, "Development of a multi-split system air conditioner for residential use," *ASHRAE Transactions* **97** (2) (1991) 127–131.

Aynur, T.N., Hwang, Y., Radermacher, R. 2006, "Field performance measurements of a VRV AC/HP system," in: *Proc. 11th Int. Refri. and Air Cond. Conf. at Purdue*.

Hai, X.H., Jun, S., Hand, Z.Y., Bin, T.C. 2006, "Design and research of the digital VRV multi-connected units with three pipes type heat recovery system," *Proc. 11th Int. Refri. Air Cond. Conf. Purdue*.

Shi, W., Shao, S., Li, X., Peng, X., Yang, X. 2003, "A network model to simulate performance of variable refrigerant volume refrigerant systems," *ASHRAE Transactions* 109 (2) (2003) 61–68.

Xia, J., Winandy, E., Georges, B., Lebrun, J. 2004, "Experimental analysis of the performances of variable refrigerant flow systems," *Building Services Engr. Research & Tech.* **25** (1) (2004) 17–23.

Choi, J.M., Kim, Y.C. 2003, "Capacity modulation of an inverter-driven multi-air conditioner using electronic expansion valves," *Energy* 28 (2) (2003) 141–155.

Hu, S.C., Yang, R.H. 2005, "Development and testing of a multi-type air conditioner without using AC inverters," *Energy Conversion and Management* 46 (3) (2005) 373–383.

Xia, J., Zhou, X., Jin, X., Wu, Y. 2003, "Simulation study on operating characteristics of multi-evaporator VRV air conditioner," in: *the 21st IIR Int. Cong. Refri*., Washington, DC, US.

Wu, C., Xingxi, Z., Shiming, D. 2005, "Development of control method and dynamic model for multi-evaporator air conditioners (MEAC)," *Energy Conv. & Mgmt.*, **46** (3): 451–465.

Zhou, Y.P., Wu, J.Y., Wang, R.Z., Shiochi, S., Li, Y.M. 2008, "Simulation and experimental validation of the variable-refrigerant-volume air-conditioning system in EnergyPlus," *Energy & Buildings*, **40**(6): 1041–1047.

Lin, J.L., Yeh, T.J. 2007, "Identification and control of multi-evaporator air conditioning systems," *Int. J. Refri.*, 30(8): 1374–1385.

Dassault Systèmes, 2015, "*Dymola Release Notes*." http://www.3ds.com/products/catia/portfolio/dymola.

Richter, C.C. 2008, "*Proposal of new object-oriented model libraries for thermodynamic systems*," Ph.D. Thesis, TU-Braunschweig, Germany.

TLK-Thermo, GmbH, 2014a, "*Engineering Services and Software for Thermal Systems*." http://www.tlk-thermo.com/index.php

TLK-Themo, GmbH, 2014b, "*Software package for visualizing thermal systems.*" http://www.tlk-thermo.com/index.php/de/dave

Joo, Y., Kang, H., Ahn, J., Lee, M., Kim, Y. 2011, "Performance characteristics of a simultaneous cooling and heating multi-heat pump at partial load conditions," *Int. J. Refri.* **34** (2011) 893-901.

Elliott, M.S., Rasmussen, B.P. 2013, "Decentralized model predictive control of a multi-evaporator air conditioning system," *Control Engineering Practice*, **21**(12), pp.1665-1677, December.

Jain, N., Koeln, J., Sundaram, S., Alleyne, A. 2014, "Partially decentralized control of large-scale variable-refrigerant-flow systems in buildings," *Journal of Process Control* **24** (2014)798-819.

Jain, N., Burns, D., Cairano, S., Laughamn, C., Bortoff, S. 2014, "Model Predictive Control of Variable Refrigerant Flow Systems" *Proc. 2014 Int. Refri. & Air Cond. Conf. at Purdue*, Paper No. 1545.

Peng, Y., Damir V., and Raymond H. "Anti-windup, bumpless, and conditioned transfer techniques for PID controllers." *IEEE Control Systems Magazine*, 16(4) (1996): 48-57.

Turner, M, and Walker, D. "Linear quadratic bumpless transfer," *Automatica* 26.8 (2000):1089-1101

Dong, L., Li, Y., Salsbury, T.I and House, J.M, *2016*, "Extremum Seeking Controls for Efficient Operation of Multi-functional Variable Refrigerant Flow System," *ASHRAE Winter Conf.*, Paper #18045, Jan. 23-27, Orlando.